CHROM. 11,300

SELECTIVE RESPONSES OF A FLAMELESS THERMIONIC DETECTOR

PAUL L. PATTERSON

Varian Instrument Division, 2700 Mitchell Drive, Walnut Creek, Calif. 94598 (U.S.A.)

SUMMARY

A flameless thermionic detector is described which uses an electrically heated bead consisting of an alkali metal compound embedded in a ceramic matrix. Measurements of detector response as a function of bead polarization voltage, bead surface temperature and composition of gaseous environment surrounding the bead demonstrate that the ionization mechanism is the thermionic emission of charged particles from the surface of the hot bead. With the bead located in a gaseous environment of air and dilute hydrogen, this detector provides highly specific responses to compounds containing nitrogen or phosphorus atoms.

INTRODUCTION

Many papers have been written about ionization detectors for gas chromatography (GC) which use alkali metal compounds to achieve specificity to samples containing nitrogen or phosphorus atoms[1,2]. Such nitrogen–phosphorus detectors have been most often referred to as either alkali flame-ionization detectors (AFID) or thermionic ionization detectors (TID). Many of the reported designs of these detectors have employed hydrogen–air flames which were sensitized by alkali metal vapors generated from an alkali metal salt bed heated by the flame itself. These flame detectors have gained the reputation of being difficult to use because of requirements for critical adjustments of gas flow-rates, unstable background signals, unstable sample responses and rapid degradation of the alkali metal salt. In recent years, considerable improvements in overall detector stability and ease of operation have been realized through the use of electrically heated beads formed from either an alkali metal–glass material[3] or a ceramic material coated with an alkali metal salt activator[4]. Such beads operate in a hydrogen–air environment, and are typically located above an orifice such that samples impinge directly on to the heated bead surface. With these electrically heated beads, it has generally been found that an enhanced nitrogen response is obtained when the hydrogen flow-rate is well below that required to provide a self-sustaining hydrogen–air flame.

In this paper there is described a flameless thermionic detector which uses a bead compound heated electrically in a manner similar to previously reported detectors. However, unlike previous detectors, the bead is·formed of an

alkali metal compound uniformly embedded throughout the body of a ceramic matrix. Such beads are capable of operating at high temperatures without melting, and exhibit good sample response characteristics even after several thousand hours of operation.

One objective of this paper is to describe a new mechanism of ionization for nitrogen–phosphorus detection. In order to understand clearly the distinction between different ionization mechanisms, it is necessary to consider carefully the terminology used to describe nitrogen–phosphorus detectors. Although it has become common for the terms AFID and TID to be used interchangeably in the GC literature, this practice is misleading because not all nitrogen–phosphorus detectors employ flames. Hence, the term AFID should clearly be restricted to only those detectors employing flames that contain alkali metal vapors. Similarly, it should be recognized that not all nitrogen–phosphorus detectors necessarily operate according to the same ionization mechanism. In the AFID, it is reasonably well established that the ionization occurs in a gas-phase process[1,2,5,6]. Heated alkali metal sources generate neutral alkali metal vapors, and specific sample responses result from chemical ionization-type reactions between the alkali metal vapor and samples. Kolb and co-workers[3,7] have argued that a similar gas-phase ionization process is active in their detector, which is flameless and uses an electrically heated bead. In the present detector, the sample actually comes into direct contact with the hot bead surface, and the possibility of a surface ionization process must also be considered. Contrary to previous uses of the term TID, it is suggested here that this term be reserved for those detectors which function according to a surface ionization process. This usage would be consistent with the conventional definition of the word "thermionic", which means the emission of electrical charge from solid surfaces that are heated[8]. It will be demonstrated that the detector in this paper satisfies this strict definition of a true thermionic detector.

EXPERIMENTAL

Instrumentation and reagents

The detector described is the thermionic detector manufactured by Varian (Palo Alto, Calif., U.S.A.). All chromatographic data were obtained using a Varian 3700 gas chromatograph with a glass column of dimensions 200 cm × 6 mm O.D. × 2 mm I.D. packed with 5% OV-101 on high-performance Gas-Chrom W, 80–100 mesh. Samples were prepared using Nanograde 2,2,4-trimethylpentane (Mallinckrodt, St. Louis, Mo., U.S.A.) as the solvent, with azobenzene (Matheson, Coleman & Bell, Norwood, Ohio, U.S.A.) and *n*-heptadecane, methyl parathion and malathion (Polyscience, Niles, Ill., U.S.A.) as the test compounds.

Alkali metal–ceramic bead

The alkali metal–ceramic bead consists of a uniform mixture of an alkali metal compound in a ceramic matrix. Embedded within the ceramic is a cylindrically-shaped electrical heating coil. When properly cured, the ceramic provides a high bond strength, non-porous surface capable of withstanding temperatures in excess of 1500°. As the alkali metal compound is distributed throughout the body of the bead, diffusional migration of the alkali metal can act to maintain an active density of alkali metal at the bead's surface layers during long-term operation.

In the present detector, the purpose of the alkali metal compound is to lower the work function of the ceramic so as to more easily allow the thermionic emission of charged particles from the surface of the heated bead. Experimentation with beads of different formulations has indicated that the work function of the bead depends on both the type and the density of the alkali metal used in the bead composition. For example, if a series of beads is constructed with equal densities of either Na, K, Rb, or Cs atoms, then the resultant bead work functions will vary in the decreasing order Na > K > Rb > Cs, which is the same order as the ionization potentials of the alkali metals. Similarly, for two beads composed of two different densities of the same alkali metal compound, the bead with the higher density will have the lower work function. It follows from these considerations that there are several different means of formulating bead compositions so as to achieve a given work function. In the present detector, it is the work function of the bead which is most important in determining the detector response, rather than the exact type of alkali metal that is used.

The determination of the optimal bead composition depends on the type of sample response desired, the bead surface temperature required to achieve that response, the ratio of sample response to background signal at that surface temperature, and the physical and chemical stability of the bead as a function of operating time. Most of the data reported were obtained with the alkali metal–ceramic bead composition that is normally supplied with the Varian detector. This bead contains Rb_2SO_4 as the alkali metal compound, and its work function is estimated in a later section. This composition was selected primarily because it provided optimal nitrogen-specific response and beads with a long operating life. The particular bead used in the present study had approximately 200 h of prior use before gathering the data reported here.

Detector configuration
Fig. 1 is a schematic illustration of the thermionic detector used. For specific nitrogen–phosphorus detection, the alkali metal–ceramic bead is positioned in a flowing gas stream composed of air, hydrogen and GC effluent. In order to heat the bead, the electrical coil embedded within the alkali metal–ceramic is connected to an adjustable, constant-current, d.c. power supply. For nitrogen–phosphorus detection, the bead is typically heated to surface temperatures of *ca.* 700–900°. The flow of gases past this hot bead then can be described as forming a gaseous boundary layer of high temperature and highly reactive chemical composition. This gaseous boundary layer probably contains flame-like radicals such as H, O and OH, which play an important role in sample decomposition and in subsequent ionization processes. Sample compounds and carrier gas eluting from the gas chromatograph are mixed with the hydrogen and are directed into the detector through the same structure used as a flame tip for a flame-ionization detector. The bead is positioned immediately above this flame tip so that incoming samples impinge directly into the gaseous boundary layer and on to the heated bead surface.

Surrounding the alkali metal–ceramic bead is a cylindrically shaped collector electrode. The collector is constructed of an open, screen-like material so as to allow a smooth, symmetrical gas flow about the bead. Electrically, the bead is biased at a voltage different from that of the surrounding collector electrode, thereby causing
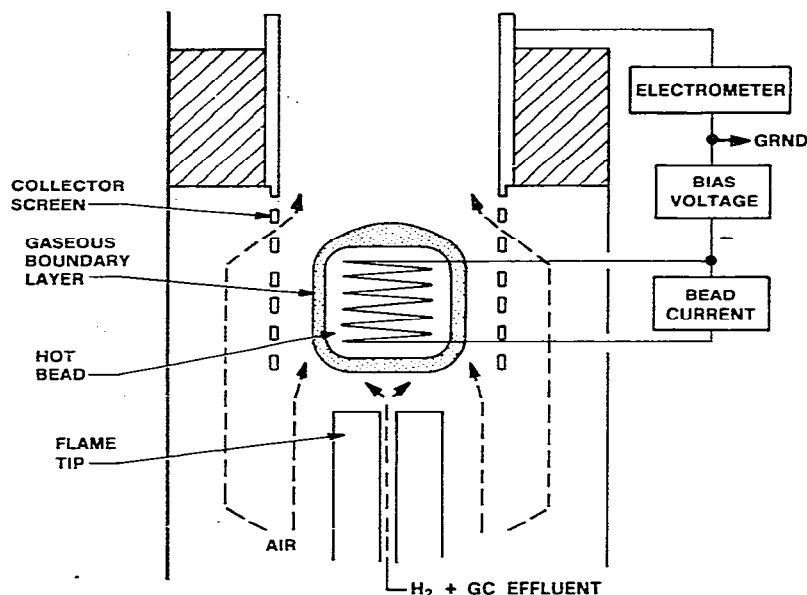
Fig. 1. Schematic diagram of the thermionic detector.

ion current to move from the bead's surface toward the collector. Ion current arriving at the collector is then measured using an electrometer. As will be shown later, the optimal sample responses occur when the bead is biased at a negative voltage, and the collector attracts negative ion current.

As shown in Fig. 1, the alkali metal–ceramic bead is located entirely within the cylindrical collector electrode. Because of this configuration, there exists a very well defined electrical field between the concentric bead and collector structures. This relative positioning of the bead with respect to the collector minimizes the requirements for precise location of the bead. In addition, it minimizes the bead voltage required to achieve efficient ion collection. In the present detector, bead bias voltages in the range 0–12 V are typically used, in contrast to the hundreds of volts employed in previously reported detectors[3,4,7].
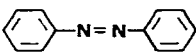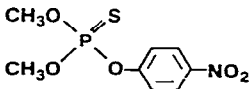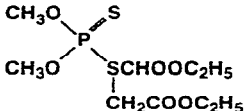
For specific nitrogen–phosphorus detection, the gas flow-rates typically supplied to the detector are 200 ml/min of air, 4.5 ml/min of hydrogen and 10–60 ml/min of GC carrier gas, which may be either helium or nitrogen. This low flow-rate of hydrogen is not sufficient to provide a self-sustaining hydrogen–air flame if the heating power to the bead is removed. The effects caused by variations in gas composition and flow-rates are thoroughly described in later sections.

Detector test sample

The thermionic detector described is an example of an element-specific detector which can be optimized for both specificity and sensitivity. In such detectors, the operating conditions that provide maximal sensitivity are not always the same as those conditions which provide maximal specificity. In evaluating the dependence of both specificity and sensitivity on various operating parameters, it is helpful to employ a test sample which contains the heteroatoms in question as well as a hydrocarbon

compound. The composition of the test sample used in the present work is described in Table I. In the data presented, the symbol I_B is used to represent the detector's background current, I_N is used to represent the current associated with the peak height of azobenzene, I_C represents the peak height of n-heptadecane and I_P represents the peak height of malathion.

TABLE I

TEST SAMPLE FOR THERMIONIC DETECTOR

Solvent: isooctane.

Compound	Structure	Compound concentration (ng/μl)	Atom concentration (ng/μl)
Azobenzene	⟨◯⟩—N=N—⟨◯⟩	3.0	0.46 (N)
n-Heptadecane	$CH_3(CH_2)_{15}CH_3$	4000	3400 (C)
Methyl parathion	CH_3O＼P⟋S CH_3O⟋ ＼O—⟨◯⟩—NO_2	2.0	0.11 (N) 0.23 (P)
Malathion	CH_3O＼P⟋S CH_3O⟋ ＼$SCHOOC_2H_5$ ｜ $CH_2COOC_2H_5$	4.0	0.38 (P)

Many of the data are displayed in relative graphs of normalized ion currents. These normalized ion currents refer to the ratios $I_B/I_B(max)$, $I_N/I_N(max)$, $I_C/I_C(max)$ or $I_P/I_P(max)$, where $I(max)$ signifies the maximal response measured for that particular graph. By displaying the data in this manner, all responses are plotted on an equivalent scale so that relative variations in each type of response can be easily compared. When varying the detector operating parameters, changes observed in the relative magnitudes of I_N, I_P and I_C are indicative of changes in specificity, while changes in the magnitudes of I_N and I_P relative to I_B are indicative of signal-to-noise variations.

Definitions of sensitivity, detectivity and specificity

The sensitivity of the detector to nitrogen atoms can be defined as follows:

S_N = peak height/N-atom flow-rate

where the peak height of the sample compound is measured in amps (A) and the N-atom flow-rate in grams of nitrogen per second (gN/sec). For a GC sample peak, the N-atom flow-rate is determined by dividing the N-weight in the sample by the peak width at half-height. In a similar way, detector sensitivities to phosphorus (S_P) and hydrocarbons (S_C) can be defined.

As will be seen later, the sensitivity of the detector can be varied over a wide range, depending on the choice of operating conditions. However, the detector background and noise also vary in a similar manner. Consequently, a better indicator of detector response is the detectivity, which is defined as follows:

$$D_N = (2 \times \text{noise})/S_N$$

where noise is measured in amps and the detectivity has the units of gN/sec. A similar definition exists for the phosphorus detectivity, D_P.

The specificity of the detector can be defined as a ratio of sensitivities. For example, the specificity of nitrogen compounds relative to hydrocarbons is defined as S_N/S_C and has the units of gC/gN. Similarly, the specificity of phosphorus compounds relative to hydrocarbons is defined as S_P/S_C and has the units of gC/gP, and the specificity of nitrogen compounds relative to phosphorus compounds is defined as S_N/S_P and has the units gP/gN.

RESULTS AND DISCUSSION

Bias voltage effects

Because of the well defined electric field existing between the bead and collector electrode, efficient collection of ionization produced at all surfaces of the bead is achieved. Consequently, effects observed as a function of bias voltage variations are not masked by extraneous losses of ionization to structures other than the collector electrode. Fig. 2 shows the variations in sample response and background current obtained when the magnitude and polarity of the bead bias voltage are changed. In general, positive voltages are characterized by very large positive background currents and negligible sample response, while negative voltages give relatively small negative background currents and relatively large negative response currents. In this detector, the crossover from negative to positive ion currents measured at the collector occurs at a bias voltage of approximately -2 V. This is because there is approximately a 2-V potential drop across the resistive coil in the bead due to the heating current. Consequently, when the top of the bead is biased at -2 V, the bottom of the bead then is actually at the same electrical potential as the collector electrode. Between bias potentials of -2 and $+2$ V, small positive current responses are obtained for both phosphorus and nitrogen, but these responses are soon masked by a rapidly increasing background current as the positive voltage increases further.

The alkali metal–ceramic bead in this detector is an abundant source of positive ion current, as is evidenced in Fig. 2 by the very large background current of $1.4 \cdot 10^{-7}$ A at $+12$ V. By comparison, the negative background current is negligible. These characteristics are not surprising, as Blewett and Jones[9] and Rice[10] described similar characteristics for alkali metal-impregnated sources many years ago. For use as a GC detector, it is clear from Fig. 2 that negative bias voltages are highly preferred because of the combination of high sample response and low
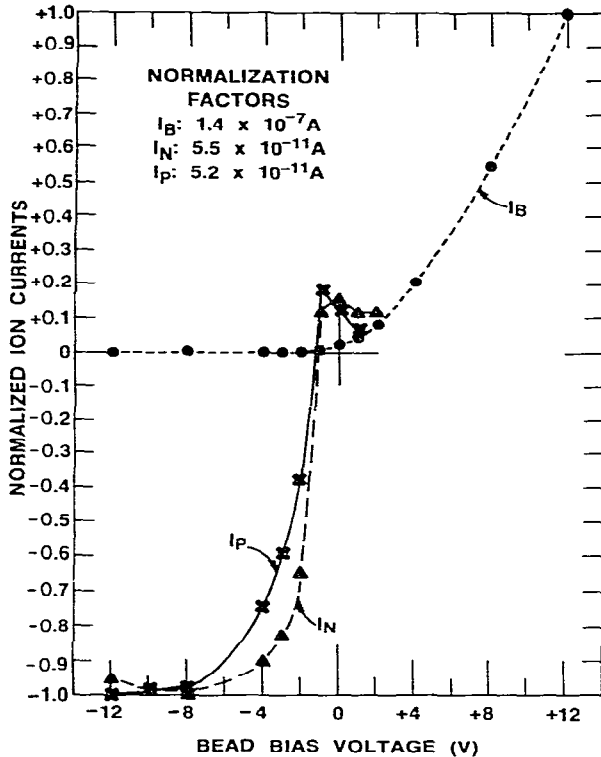
Fig. 2. Variations of background current (I_B), nitrogen response current (I_N) and phosphorus response current (I_P) as a function of bead bias voltage.

background current. Therefore, all of the remaining data reported were obtained at bias voltages in the range -4 to -12 V.

The data in Fig. 2 also demonstrate that the mechanism of ionization in the detector is a surface ionization process. If the ionization occurred in the gas phase, then equal concentrations of positive and negative gas phase ions would be created. In that event, the graphs of current at positive and negative bias voltages would be reasonably symmetric, mirror images. That is clearly not the case. The graphs of both background and response currents are highly asymmetric with respect to opposite polarities of the bias voltage. That type of behavior can occur only if the currents measured are arising by emission of charged particles from the bead itself. Therefore, the detector operates by sensing changes in the magnitude of negative ion current emitted from the surface of the heated alkali metal–ceramic bead.

Bead surface temperature effects

The surface temperature (T_B) of the alkali metal–ceramic bead depends on the bead heating current (i), the composition of gases surrounding the bead, the flow-rate (F) of gases past the bead and the detector wall temperature (T_D). These dependences can best be understood by using an equation balancing heat input and losses from the theory of thermal conductivity detectors[11], as follows:

$$i^2R = (a_1\lambda + a_2FC_p)(T_B - T_D) \tag{1}$$

where R is the electrical resistance of the heating coil in the bead, λ is the thermal conductivity of the gas mixture around the bead, C_p is the specific heat of the gas mixture and a_1 and a_2 are constants. Eq. 1 can be rewritten as

$$T_B = i^2 a_3 + T_D \tag{2}$$

where

$$a_3 = R/(a_1\lambda + a_2 F C_p)$$

In the preceding section, it was concluded that the ionization process in the detector involved the emission of negative ion current from the heated alkali metal–ceramic bead. According to the well known Richardson–Dushman equation[12], the thermionic emission current from a hot surface is proportional to an exponential factor containing the surface temperature:

$$I \propto e^{-W/T_B}$$

where I is the emitted current and W is the electronic work function of the hot alkali metal–ceramic bead. Consequently, the logarithm of I satisfies the following relationship:

$$\ln I \propto -W/T_B \tag{3}$$

From eqn. 2, the factor $1/T_B$ can be expressed as

$$1/T_B = (1/i^2 a_3)(1 + T_D/i^2 a_3)^{-1} \tag{4}$$

For typical nitrogen–phosphorus detection, T_B is in the range 700–900° and T_D is in the range 150–350°, so that $T_D/i^2 a_3$ is usually less than unity. Therefore, the factor $(1 + T_D/i^2 a_3)^{-1}$ can be approximated by $(1 - T_D/i^2 a_3)$ and eqn. 4 becomes the approximate relationship

$$1/T_B = (1/i^2 a_3)(1 - T_D/i^2 a_3) \tag{5}$$

Substituting eqn. 5 into relation 3 then gives the following approximate expressions:

$$\ln I \propto -W/i^2 a_3 \tag{6}$$

for variations in i with T_D held constant, and

$$\ln I \propto W T_D/i^4 a_3^2 + \text{constant} \tag{7}$$

for variations in T_D with i held constant. From relations 6 and 7, it is predicted that graphs of $\ln I$ versus i^{-2} and $\ln I$ versus T_D should be straight lines with slopes proportional to the work function, W.

Fig. 3 shows the variations of I_B, I_N and I_P plotted on a linear scale against bead current, i, and on a logarithmic scale as a function of i^{-2}. Fig. 4 shows similar graphs of I_B and I_N plotted on both linear and logarithmic scales against detector temperature. The logarithmic plots in both Figs. 3 and 4 exhibit the straight-line fit of the data predicted by relations 6 and 7. Hence, both the background and response currents exhibit the dependence on bead surface temperature that is expected for the process of thermionic emission. Further, the difference in slopes of the graphs of response current and background current demonstrates that the response
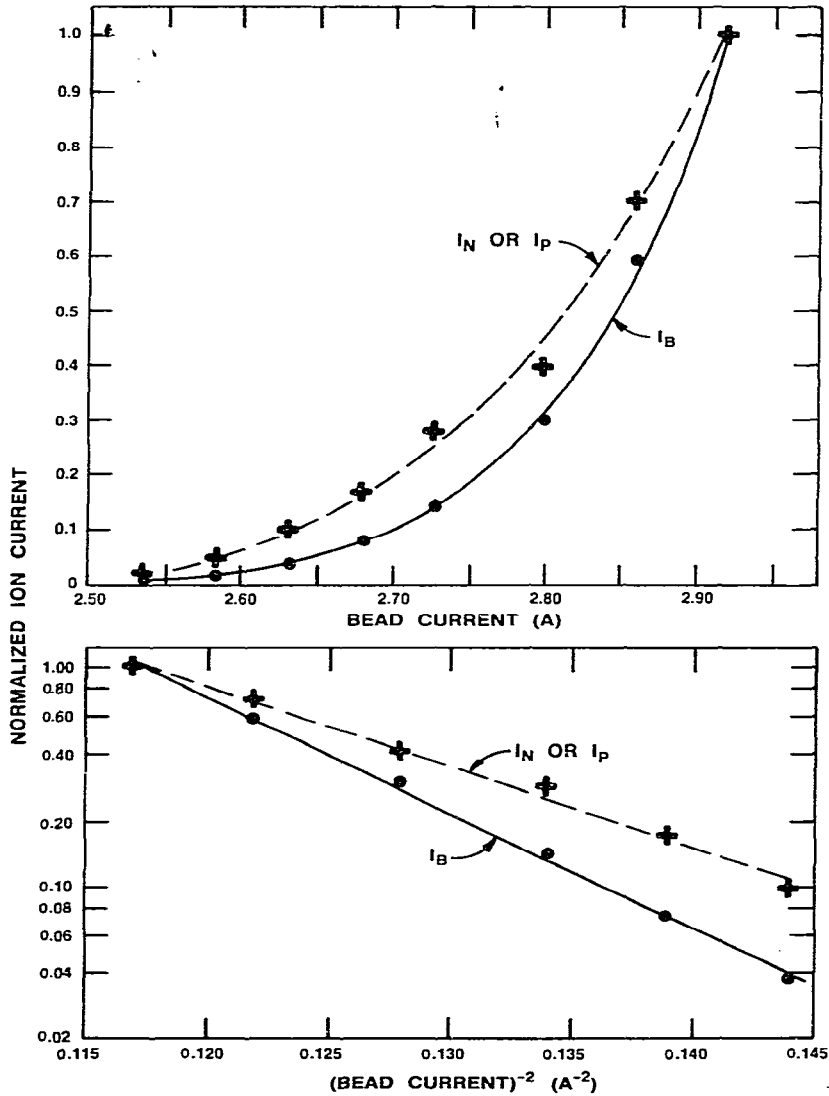

Fig. 3. Variations of I_B, I_N and I_P as a function of bead heating current and (bead heating current)$^{-2}$. In the top graph the ion current scale is linear and in the bottom graph it is logarithmic.
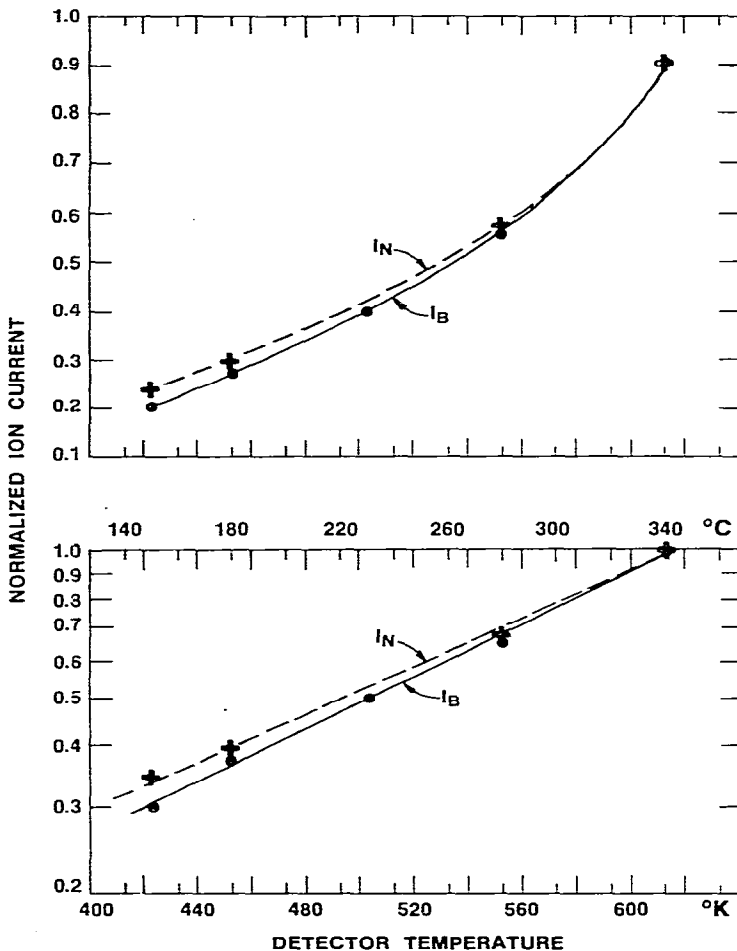
Fig. 4. Variations of I_B and I_N as a function of detector temperature at constant bead heating current. In the top graph the ion current scale is linear and in the bottom graph it is logarithmic. I_N refers to nicotine response rather than azobenzene.

current can be viewed as being caused by an effective reduction of the work function of the bead at those instances when the bead's surface is exposed to the nitrogen- or phosphorus-containing samples.

From the combined data in Figs. 3 and 4, it can be calculated that the bead's work function in the absence of samples is approximately 3.4 eV, whereas in the presence of nitrogen or phosphorus compounds it is reduced to about 2.3 eV. This reduction of the work function can be explained by postulating that the reactive chemical environment of the gaseous boundary layer is favorable for the formation of highly electronegative decomposition products from the nitrogen or phosphorus sample compounds. These electronegative species subsequently can form gaseous negative ions by extracting electrons from the surface of the heated alkali metal-ceramic bead[12]. Although the exact identities of these electronegative decomposition

products have not been established, probable species such as CN, NO_2 and PO_2 are all known to be highly electronegative.

In Fig. 3 it is indicated that both I_N and I_P have the same dependence on bead current. Actually, the GC peak heights of all of the compounds in the test sample maintain approximately the same relative magnitudes over the range of bead current variations described in Fig. 3. Hence, it can be concluded that the specificity of this detector to nitrogen and phosphorus compounds is reasonably insensitive to variations in bead surface temperature provided that the temperature is high enough to initiate decomposition of the samples. At the same time, the absolute magnitudes of the peak heights in the test chromatograms are a strong function of bead surface temperature, as indicated in the plots in both Figs. 3 and 4. Consequently, the sample sensitivity of this detector can be adjusted over a wide range by varying the bead heating current. However, a comparison of the response and background currents plotted in Fig. 3 shows that the background current in this detector increases at a faster rate with increasing bead temperature than does the sample response. Therefore, the higher the bead temperature is, the greater the sample response will be, but at the cost of a decrease in the ratio of sample response to background current. As a general rule, then, it appears to be best to operate this detector at as low a bead surface temperature as is consistent with the type of sample response desired as well as with the noise limitations of the electrometer used to measure currents. More specifically, optimal operation of the detector is achieved at bead heating currents that produce a bead noise level which is about a factor of two greater than the basic electrometer noise. In the present detector, that bead noise level is typically $0.5 \cdot 10^{-14}$–$1.0 \cdot 10^{-14}$ A. Higher bead currents give higher sample response, but also higher noise.

Fig. 5 illustrates the dependence of detector background current on air flow-rate and on carrier gas flow-rate for both helium and nitrogen carrier gases. These data were obtained by using a constant bead heating current. Sample response variations would be qualitatively similar to the variations in I_B as the dependences exhibited in Fig. 5 are primarily the result of bead surface temperature changes. With nitrogen as the carrier gas, the effects illustrated in Fig. 5 are mainly caused by changes in the convective heat losses from the bead as represented by the a_2FC_p term in eqn. 1. With helium as the carrier gas, the effects illustrated in Fig. 5 represent changes in thermal conductivity heat losses as represented by the $a_1\lambda$ term in eqn. 1, as well as changes in the convective heat losses. Generally, any change in bead temperature resulting from a change in gas flow-rate can always be counteracted by a readjustment of the bead heating current. For example, if the carrier gas is changed from helium to an identical flow-rate of nitrogen, then the bead heating current is decreased to give a constant I_B, and the resulting test chromatogram then reveals the same sample response for nitrogen as it was for helium.

For previous detectors using electrically heated alkali metal–glass beads, Hartigan et al.[13] reported similar data on background current versus air flow-rate, and Lubkowitz et al.[14] reported a similar dependence of background current on nitrogen carrier gas flow-rate. Based on their observations, Lubkowitz et al. concluded that their thermionic detector was a concentration-sensitive detector rather than a mass flow-sensitive detector. However, as already discussed, the dependence of background and response on carrier gas flow-rate is caused mainly by changes in
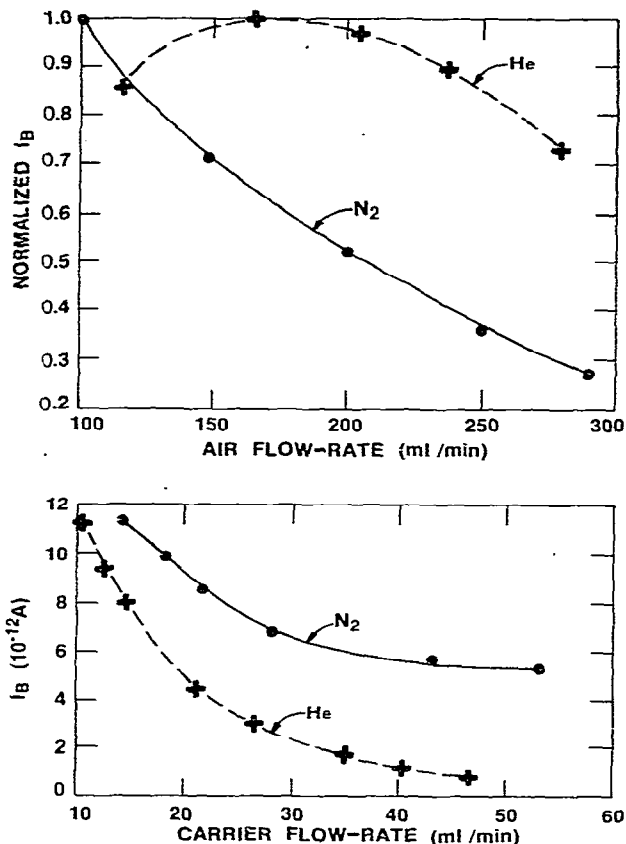
Fig. 5. Variations of I_B at constant bead heating current as a function of air flow-rate and carrier gas flow-rate for both N₂ and He carrier gases. In the air flow-rate graph the He and N₂ flow-rates were 25 ml/min; in the carrier gas flow-rate graph the air flow-rate was 200 ml/min.

bead surface temperature. If the bead heating current is adjusted to maintain a constant bead temperature, as indicated by a constant I_B, then it is found that these detectors behave appropriately as mass flow-sensitive detectors.

Effects of gas boundary layer composition

It is well known that the thermionic emission of charge from a hot surface can be strongly influenced by the type of gaseous atmosphere prevailing at that surface. Consequently, it is not surprising that the specificity of the present detector is found to be strongly dependent on the composition of the gaseous boundary layer surrounding the alkali metal–ceramic bead. With air and hydrogen both supplied to the detector, the composition of reactive species in the boundary layer is most strongly influenced by the flow-rate of hydrogen. Fig. 6 shows a series of test sample chromatograms obtained at three different hydrogen flow-rates. The chromatogram at 4.2 ml/min represents the response obtained for the conditions normally used for specific nitrogen or phosphorus detection. When the hydrogen flow-rate is increased to 7.2 ml/min, it is seen that significant decreases in specificity of azobenzene relative
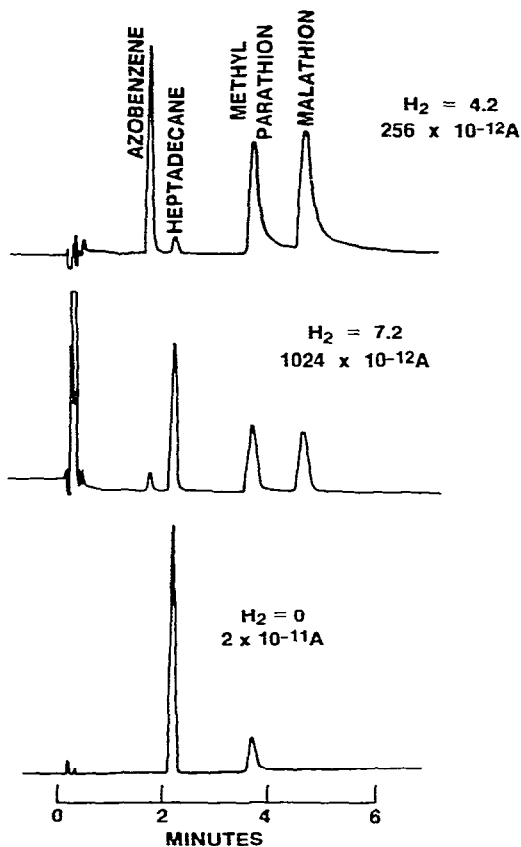
Fig. 6. Chromatograms of detector test sample at different H_2 flow-rates and constant bead heating current. H_2 flow-rates in ml/min. GC conditions: carrier gas, He; flow-rate, 25 ml/min; column temperature, 205°; injector temperature, 210°; detector temperature, 250°.

to *n*-heptadecane, methyl parathion and malathion occur, as well as decreases in the specificity of methyl parathion and malathion relative to *n*-heptadecane. When the hydrogen is turned off, it is seen that response is no longer obtained for azobenzene and malathion.

Fig. 7 shows the variations in I_B, I_N, I_C and I_P as a function of hydrogen flow-rate for both nitrogen and helium carrier gases. Compared with the flow-rates of air and carrier gas, the hydrogen flow-rates represented are very low. Consequently, these variations in hydrogen flow-rate had only a very small effect on the surface temperature of the alkali metal–ceramic bead, as was evidenced by the fact that the bead glowed at the same color temperature throughout these variations. This means that the effects exhibited in Fig. 7 are caused mainly by changes in the chemical composition of the gaseous boundary layer. In particular, it seems reasonable to assume that the main action of variations in hydrogen flow-rate is to change the concentrations of the radicals H, O and OH in the boundary layer.

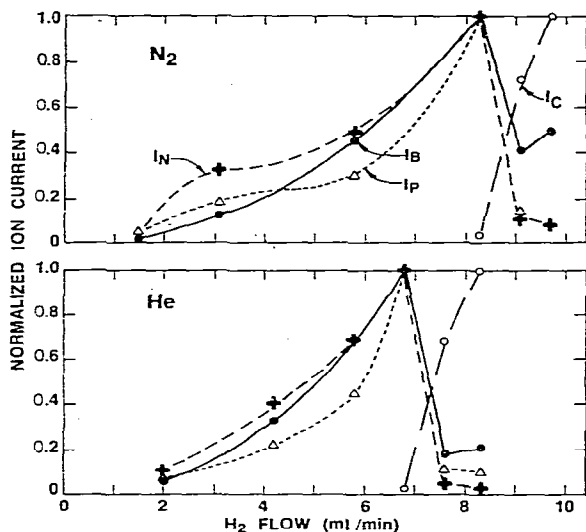Between 1.5 and 8.3 ml/min of hydrogen for nitrogen carrier gas and 2.0 and

Fig. 7. Variations in I_B, I_N, I_P and hydrocarbon response current (I_C) as a function of H_2 flow-rate for He and N_2 carrier gases at 25 ml/min. Bead heating current held constant.

6.8 ml/min of hydrogen for helium carrier gas, this detector exhibits a high specificity to both nitrogen and phosphorus compounds relative to hydrocarbons. In the same ranges of hydrogen flow-rate, I_B varies as the square of hydrogen flow-rate to a very good approximation. Above hydrogen flow-rates of about 8.3 ml/min for nitrogen carrier gas, and 6.8 ml/min for helium carrier gas, there abrupt decreases in I_B, I_N and I_P and a large increase in I_C occur. These discontinuities appear to be associated with the onset of a new stage of ignition of the hydrogen–air mixture. At hydrogen flow-rates greater than these ignition points, specificity to nitrogen and phosphorus compounds is rapidly lost.

Bead composition effects

The emission of negative charge from the alkali metal–ceramic bead of the detector depends on the work function of the bead as well as the surface temperature of the bead. The surface temperature also is important in determining the type of decomposition products formed from sample compounds. Consequently, a certain degree of enhanced sensitivity and specificity is possible by choosing the bead composition to give the best sample response at the desired operating temperature. For example, if the desired response requires a high surface temperature for the preferred decomposition chemistry, then a bead of relatively low work function may provide too large a background current in comparison with the sample current. In that event, a better response is obtained by using a bead composition of higher work function. Similarly, it is expected that specific responses requiring relatively low surface temperatures will also be best obtained by using bead compositions of relatively low work function.

An example of data obtained from alkali metal–ceramic beads of two different compositions is shown in Fig. 8. For this illustration, the beads were operated in
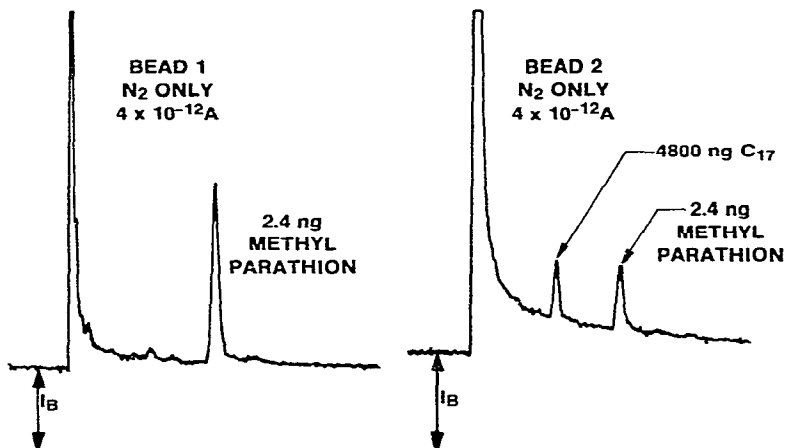
Fig. 8. Chromatograms of detector test sample for beads of different composition. Bead 1 has a ower work function than bead 2. Both beads operated in inert N_2 environment.

a chemically inert environment of pure nitrogen. In this instance, any electronegative species present in the gaseous boundary layer of the bead must be formed from the thermal decomposition chemistry involving the constituent atoms of the sample itself. In this mode of operation, the detector provides a highly specific response to compounds containing an electronegative NO_2 group such as methyl parathion in the test sample. For the data shown in Fig. 8, bead 1 contained cesium and had a lower work function than did bead 2, which contained rubidium. Consequently, when the heating current to each bead was adjusted to give equal magnitudes of I_B, the resultant surface temperature of bead 2 was significantly higher than that of bead 1. In this instance, it is seen in Fig. 8 that bead 1 provides an improvement in both sensitivity and specificity to methyl parathion in comparison to bead 2.

Performance specifications for nitrogen–phosphorus detection

For specific detection of nitrogen or phosphorus compounds, the detector has the capability of responding to samples at the picogram level, as illustrated in Fig. 9. In the present work, the detectivity for nitrogen in azobenzene was determined to be $D_N = 5 \cdot 10^{-14}$ gN/sec, while the detectivity for phosphorus in malathion was $D_P = 2.5 \cdot 10^{-14}$ gP/sec.

The peak-height sensitivities, S_N and S_P, are plotted as a function of N- and P-atom flow-rates in Fig. 10. For nitrogen, the response was linear over a range of 10^5 in N-atom flow-rate, while for phosphorus the response was linear over an approximate range of 10^4 in P-atom flow-rate. For the operating conditions used in Fig. 10, the sensitivity S_N was 0.2 A/gN/sec, while S_P was 0.4 A/gP/sec. Under the same conditions, the sensitivity S_C to carbon in *n*-heptadecane was $3 \cdot 10^{-6}$ A/ gC/sec. Consequently, the specificity ratios of this detector were as follows:

$$S_N/S_C = 7 \cdot 10^4 \text{ gC/gN}$$
$$S_P/S_C = 10^5 \text{ gC/gP}$$
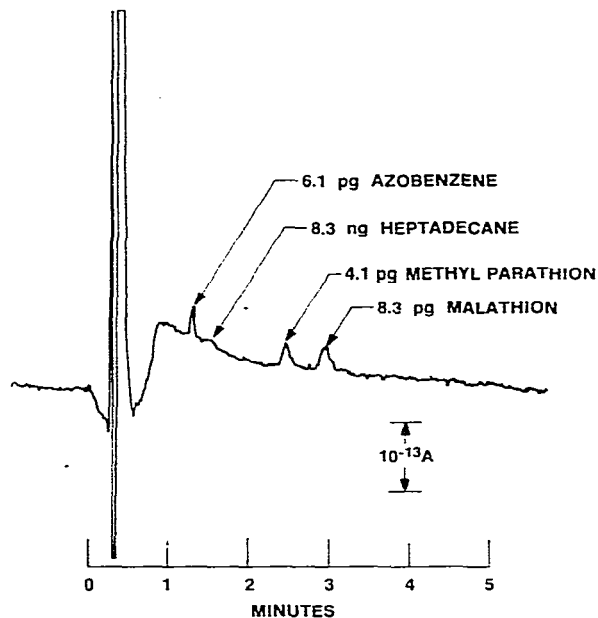$$S_N/S_P = 0.5 \text{ gP/gN}$$

Fig. 9. Chromatogram illustrating picogram-level detectivity for nitrogen and phosphorus compounds. GC conditions: carrier gas, He; flow-rate, 25 ml/min; column temperature, 220°; injector temperature, 220°; detector temperature, 300°.
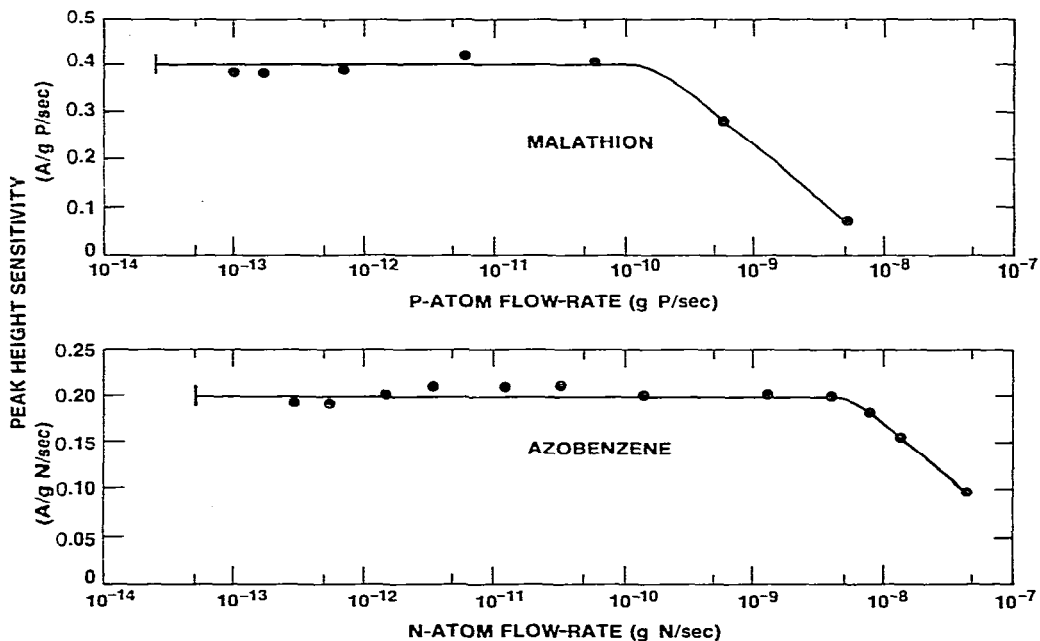

Fig. 10. Plot of phosphorus sensitivity and nitrogen sensitivity as a function of P-atom and N-atom flow-rates.

CONCLUSIONS

The detector described functions according to the process of thermionic emission of negative charge from the surface of a heated alkali metal–ceramic bead. Sample compounds are directed to impact on the bead's surface, and the presence of certain types of sample compounds is indicated by the enhanced emission of charge from the bead. The most critical parameters determining the response of this detector are the bead composition, the bead surface temperature and the composition of the gaseous environment surrounding the bead's surface. The bead surface temperature and the composition of the gaseous environment determine the gaseous products formed from the decomposition of sample compounds. The composition of the bead and the bead surface temperature determine the negative charge emission characteristics of the bead.

REFERENCES

1 V. V. Brazhnikov, M. V. Gur'ev and K. I. Sakodynsky, *Chromatogr. Rev.*, 12 (1970) 1.
2 D. J. David, *Gas Chromatographic Detectors*, Wiley, New York, 1974, Ch. 5.
3 B. Kolb and J. Bischoff, *J. Chromatogr. Sci.*, 12 (1974) 625.
4 C. A. Burgett, D. H. Smith and H. B. Bente, *J. Chromatogr.*, 134 (1977) 57.
5 F. M. Page and D. E. Woolley, *Anal. Chem.*, 40 (1968) 210.
6 J. Sevcik, *Chromatographia*, 6 (1973) 139.
7 B. Kolb, M. Auer and P. Pospisil, *J. Chromatogr. Sci.*, 15 (1977) 53.
8 W. C. Michels (Editor), *The International Dictionary of Physics and Electronics*, Van Nostrand, Princeton, N. J., 2nd ed., 1961.
9 J. P. Blewett and E. J. Jones, *Phys. Rev.*, 50 (1936) 464.
10 C. W. Rice, *U.S. Pat.*, 2,550,498 (1951).
11 A. E. Lawson, Jr. and J. M. Miller, *J. Gas Chromatogr.*, 4 (1966) 273.
12 E. W. McDaniel, *Collision Phenomena in Ionized Gases*, Wiley, New York, 1964, Ch. 13.
13 M. J. Hartigan, J. E. Purcell, M. Novotny. M. L. McConnell and M. L. Lee. *J. Chromatogr.*, 99 (1974) 339.
14 J. A. Lubkowitz, J. L. Glajch, B. P. Semonian and L. B. Rogers, *J. Chromatogr.*, 133 (1977) 37.